

Received February 9, 2021, accepted February 22, 2021, date of publication March 9, 2021, date of current version March 29, 2021.

Digital Object Identifier 10.1109/ACCESS.2021.3064885

Precise Burden Charging Operation During Iron-Making Process in Blast Furnace

HAIGANG ZHANG¹, (Member, IEEE), SHAOLUN SUN², (Member, IEEE),
AND SEN ZHANG¹, (Member, IEEE)

¹Institute of Applied Artificial Intelligence of the Guangdong-Hong Kong-Macao Greater Bay Area, Shenzhen Polytechnic, Shenzhen 518055, China

²School of Automation and Electrical Engineering, University of Science and Technology Beijing 100083, China

Corresponding author: Sen Zhang (zhangsen@ustb.edu.cn)

This work was supported in part by the National Natural Science Foundation of China under Grant 61806208, in part by the General Higher Education Project of Guangdong Provincial Education Department under Grant 2020ZDZX3083, in part by the Rural Science and Technology Commissioner Project of Guangdong Provincial Science and Technology Department under Grant KPT20200220, Natural Science Foundation of Guangdong Province under Grant 2019A1515011267, and in part by the Shenzhen basic research project under Grant JCYJ20190809113617119.

ABSTRACT The burden charging operation in blast furnace is one of the most important operations during iron-making process. In this paper, we focus on the study of precise burden charging operation, which involves two aspects: How to obtain and form the optimal burden surface shape. For the first problem, we construct a mapping model between the burden surface characteristic parameters and the comprehensive operational performance indicators of the blast furnace, and transform the search of optimal burden surface shape into the target optimization problem. The second problem refers to establishing a suitable burden charging strategy based on the basic burden surface and the optimal burden surface. In our work, by adaptively adjusting the opening degree of the throttle valve, it is possible to control accurate burden volume during the rotation of the charging chute, which can make sure to spill the appropriate burden volume on the suitable charging units. In the simulation of experiments, we collected the real industrial data during iron-making process and demonstrated the efficiency of the proposed model.


INDEX TERMS Bell-less top blast furnace, burden optimal model, precise charging strategy, multi-objective optimization.

I. INTRODUCTION

The iron and steel industry is a pillar industry of the national economy in China, of which the ironmaking process in blast furnace is the most important component. Blast furnace (BF) contains a lot of complex physical and chemical reactions during ironmaking process [1] Fig. 1 presents a simple schematic diagram for the production of hot metal in BF. There are two kinds of material movements inside the BF. The solid raw materials including the ore and coke are charged based on the bell-less top feeding system from the top of BF, while the hot air, sometimes with some auxiliary fuels like the oxygen and pulverized coal is equipped through the bottom tuyeres and up to the hearth [2]–[4] The thermochemical reduction of iron oxide ore by carbon monoxide is the main principle inside the BF. The continuous and stable thermal

environment is the prerequisite for the production of molten iron [5], [6] The operating mechanism of ironmaking process often has the characteristic of nonlinearity, large time delay, serious noise and distributed parameters, resulting the control methods, especially for the burden charging operation, are mainly based on the experience. The automatic control of BF ironmaking process is a hot topic in the academic and industrial research [7], [8].

The burden charging operation is very important during iron-making process in BF [9], [10] The most commonly used charging way is the bell-less charging operation. After being feeded into the parallel or serial hoppers, the ore and coke would be sown layer by layer through the rotating chute [11], [12] The burden surface shape can directly affect the gas flow distribution during iron-making process [13]. In general, the V-type burden surface with suitable platform is beneficial and can satisfy the criterion of the development of gas flow: making the center gas flow active and the marginal

The associate editor coordinating the review of this manuscript and approving it for publication was Danilo Pelusi .

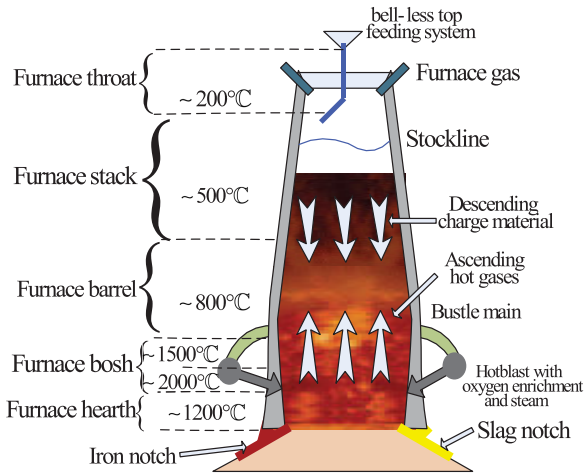


FIGURE 1. Blast furnace.

gas flow suppressive [14] However, the research of optimal burden surface shape is seldom. The burden surface shape and the operating status of BF are closely related. It is reasonable to transform the search of optimal burden surface shape into the multi-objective optimization problem of comprehensive operational performance indicators in BF production.

The multi-objective optimization problem of iron-making process in BF has drawn attention of the research in industry and academia. Liu made the constructal design of the BF and regarded it as a multi-objective optimization problem [15] The optimization function is integrated with hot metal yield and useful energy. The optimization variables are some production parameters, like the oxygen enrichment and operation temperature *et al.* Helle designed the top gas recycling strategy in order to reduce the carbon dioxide content in the atmosphere [16] Considering the conflicting goals of reducing both production costs and emissions, the strategy can be formulated as a multi-objective optimization problem. Hua *et al.* established the optimization model for the ingredient during BF production based on NSGA-II algorithm [17] The goal is to reduce the production cost and CO_2 emissions. The research about the optimal burden surface shape and charging strategy is seldom. Watakabe *et al.* proposed a high ratio coke mixed charging technique in the JFE technical report [18] Zhou *et al.* introduced an intelligent charging system, which makes real-time adjustment for the throttle opening degree after calculating the error between the real and ideal burden surfaces [19] However, they have not proposed the method to determine the shape of optimal burden surface, while the operability of the strategy is not strong.

In this paper, we focus on two contributions refer to the charging operation during iron-making process. The first is the multi-objective optimization model for the burden surface shape, where three premises are put forward: (1) The pursuit of stability is the main element during BF production. The optimal burden surface cannot destroy the production balance in BF. (2) There exists great differences for the volume, production time, operating habit *et al.* in different BFs.

Thus the optimal burden surface shape is not unique. (3) There are various operating statuses during iron-making process in BF. It should set different optimal burden shapes for different production statuses. Thus the optimal burden surface shape is dynamic and variable. The second contribution is the design of precise charging strategy based on the online adjustment of the throttle opening degree. The throttle opening degree can affect the burden volume per unit time. During the process of rotating charging operation, the adjustment of throttle opening degree can make sure to spill the appropriate volume of the burden on the suitable area. It should be mentioned that the complexity and opacity of BF production indicate that the shape of the burden surface is not the only factor affecting the production status of BF. Our work opens up a new idea for the smart production of iron-making process in BF. More details about these two innovations are as follows.

(1) In this paper, Extreme Learning Machine(ELM) algorithm [20] is applied to establish the prediction model for the operating performance indexes. The model inputs are the features of burden surface, while the performance index is a comprehensive indicator, which contains various variables that react to the production status of BF. Then the Differential Evolution (DE) algorithm [21] optimizes the prediction model and searches the optimal burden surface shape.

(2) During the charging process, the rotating chute evenly spread the solid raw materials on the basic surface. With the change of the inclination angle of the chute, the burden can cover the entire surface. According to the charging mathematical model, we can calculate the falling points of burden. The concept of 'charging unit' is proposed based on the ring partition for the basic burden surface. Then the required volume on different charging units can be calculated, while the corresponding throttle opening degrees can be obtained.

It is necessary to explain why the ELM algorithm is used for establishing the prediction model. ELM algorithm is a general neural network framework for regression and classification problems. Thanks to the random selection of hidden node weights, its most prominent advantage is fast training and inference speed, which is very suitable for iron-making production in BFs that emphasizes timeliness. In addition, there have been many references [20] showing that ELM is superior to other traditional algorithms, such as SVM, BP, etc. in term of generalization ability. Last but not least, it is inappropriate or unreasonable to employ more powerful machine learning algorithm, such as deep learning framework like CNN or RNN. Based on the 2D definition model for the burden surface, we abstract the burden shape into 7 features, and ELM algorithm can well deal with low-dimensional feature data.

The paper is organized as follows: Section II presents the optimal model for burden surface, including the introduction of ELM algorithm and the DE optimization method. Section III introduces the charging strategy, including the array radar detection technology and the throttle opening model. Simulation results are presented in Section IV, while

Section V gives the conclusion and future work of our paper.

II. MODELING OF OPTIMAL BURDEN SURFACE

In this section, we establish the optimal model for the shape of burden surface. ELM algorithm is applied to establish the relationship model between the burden surface and the production indexes. Then DE optimization algorithm searches for the optimal shape of burden surface based on the improvement of production indexes.

A. EXTREME LEARNING MACHINE

The ELM algorithm was originally proposed by Huang subject to a general single hidden layer network. ELM gets rid of human tuning with random initialization of learning parameters. Then the output weights can be determined by the theory of least square method [20], and [22]

Given a training set consisting of N arbitrary distinct samples $S = \{(x_i, t_i) | x_i \in R^n, t_i \in R^m, i = 1, 2, \dots, N\}$, the network function with \tilde{N} hidden nodes can be formulated as

$$f_{\tilde{N}} = \sum_{j=1}^{\tilde{N}} \beta_j G(a_j, b_j, x_i) = t_i, \quad i = 1, 2, \dots, N \quad (1)$$

where a_j and b_j are the learning parameters which will be determined randomly. β_j is the output weight matrix connecting the j th hidden and the output nodes. x_i and t_i are the feature and output of the i th observation respectively. $G(a_j, b_j, x_i)$ is a nonlinear piecewise continuous function which satisfies ELM universal approximation capability theorems [23]

The above \tilde{N} equations can be written in the matrix form as

$$H\beta = T \quad (2)$$

where $H = \begin{bmatrix} G(a_1, b_1, x_1) & \dots & G(a_{\tilde{N}}, b_{\tilde{N}}, x_1) \\ \vdots & \ddots & \vdots \\ G(a_1, b_1, x_N) & \dots & G(a_{\tilde{N}}, b_{\tilde{N}}, x_N) \end{bmatrix}_{N \times \tilde{N}}$ is called output hidden layer matrix.

After the fixed nonlinear transformation with no adjustable learning parameters, the hidden layer of ELM network maps the input space onto a new linear space, named ELM feature space [23] The ELM model with a single-output node can be formulated as the following optimization problem:

$$\begin{aligned} \text{minimize } J_{ELM} &= \frac{1}{2} \|\beta\|^2 + C \frac{1}{2} \sum_{i=1}^N \|e_i\|^2 \\ \text{subject to : } & h(x_i)\beta = t_i - e_i \end{aligned} \quad (3)$$

where e_i represents the training error of the i th observation. $h(x_i)$ is the i th row of output hidden layer matrix. C is a use-specified parameter and it can provide a trade-off between the training error and the norm of the output weights.

According to the Karush-Kuhn-Tucker(KKT) theory [24], the above ELM model is equivalent to solving the following

dual optimization problem:

$$\begin{aligned} L_{ELM} &= \frac{1}{2} \|\beta\|^2 + C \frac{1}{2} \sum_{i=1}^N \|e_i\|^2 \\ &\quad - \sum_{i=1}^N \sum_{j=1}^m \tau_{ij} (h(x_i)\beta_j - t_{ij} + e_{ij}) \end{aligned} \quad (4)$$

Then one can get

$$\nabla_{ELM} = \beta + CH^T (T - H\beta) = 0 \quad (5)$$

Then the output weights can be estimated as follows:

$$\hat{\beta} = \left(\frac{I_{\tilde{N}}}{C} + H^T H \right)^{-1} H^T T \quad (6)$$

where $I_{\tilde{N}}$ is an identity matrix with dimension \tilde{N} .

The biggest advantage of the ELM algorithm is the fast training speed. Here we present the discuss of cost effectiveness of ELM algorithm. For the basic ELM framework, it contains the calculation of hidden layer output matrix and the calculation of output weights. The time complexity of the calculation of hidden layer output matrix H is $O(2 * n * m * \tilde{N})$; the time complexity of the calculation of $H^T H$ is $O(\tilde{N}^2 * n)$; the time complexity of the calculation of output weights is $O(\tilde{N}^3) + O(\tilde{N}^2 * n^2)$, where n and \tilde{N} are presented in Section 2.2. So the total time complexity of the basic ELM algorithm is $O(2 * n * m * \tilde{N}) + O(\tilde{N}^2 * n) + O(\tilde{N}^3) + O(\tilde{N}^2 * n^2)$. Fast training and reasoning time can ensure the timeliness of algorithm implementation.

B. DIFFERENTIAL EVOLUTION ALGORITHM

Differential Evolution (DE) algorithm is a parallel direct search method, which can minimize the function in linear, non-differential and continuous space [25] Compared with the traditional genetic algorithm, they have similarities and differences. DE algorithm also depends on the manipulation and efficiency of three main operators: mutation, crossover and selection. DE algorithm preserves the population-based global search strategy, which reduces the complexity of genetic operations by employing real-coded, differential-based mutation operation and one-to-one competitive survival strategies. DE algorithm has been applied in many fields, such as artificial neural network, chemical electrical, mechanical design, bioinformatics *et al.* [26]

Fig. 2 presents the scheme of DE optimization algorithm. DE starts with a population of NP candidate solutions which may be represented as $X_{i,G}, i = 1, 2, \dots, NP$, where i index denotes the population and G denotes the generation to which the population belongs. The initial vector population is chosen randomly, which should cover the entire parameter space. Then DE selects the differences vector of any two individuals as a basic individual in the initial population, while the remaining individuals are selected as the reference individuals. DE generates the new parameter vectors by

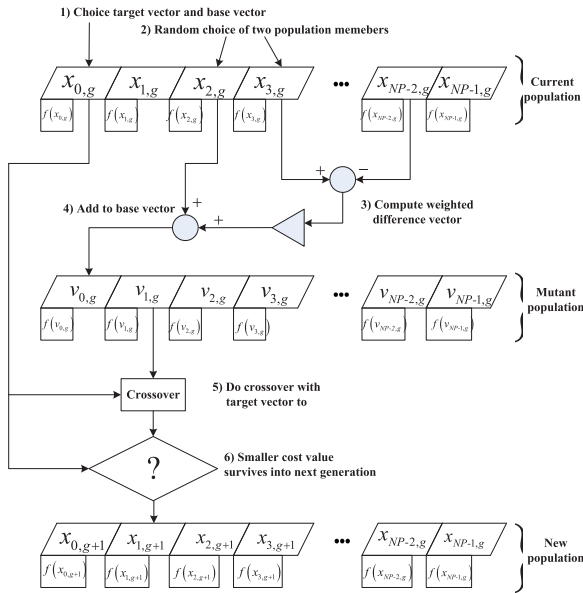


FIGURE 2. DE algorithm.

adding the difference vector weighted by the certain rules to a third vector. This operation is called mutation. Then the trial vector is generated after mixing the mutated vector with the parameters of another predetermined vector, which is the main idea in crossover operation. The last operation is called selection, in which DE chooses the better parameter vector with lower cost function between the trial vector and target vector in the following generation [27] DE algorithm is employed to make optimization for the prediction model of performance index in BF production. The optimized objects are the features of burden surface.

C. OPTIMIZATION MODEL FOR BURDEN SURFACE

In this subsection, we establish the optimization model for the burden surface of BF based on the ELM algorithm and DE algorithm. In order to better describe the shape of the burden surface, we establish the feature extraction model for the 2D burden surface, as shown in Fig. 3. The coordinate system is set at the position of zero line near the BF throat. Zero line is the x -axis, while the centerline in BF body is the y -axis with down direction. Seven features are extracted to represent the burden line, such that the distance between the burden line and the zero position h_1 , the depth of the hopper h_2 , the width of the hopper l_1 , the width of the platform l_2 , the slop angle of the hopper α , the central angle of the hopper β and the slope angle of edge region γ . The seven features are consistent with the cognition of the operators to the burden line. They will be employed in the optimization process of burden surface.

Fig. 4 presents the optimization model for the burden line. First, the regression model between the features of burden line and the performance index of iron-making process is established by ELM algorithm. The radial ratio between the ore and coke can represent the distribution change of burden, which is also the input of prediction model. As we all known,

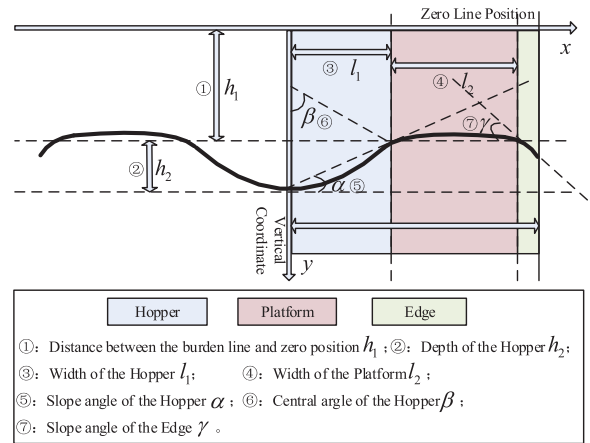


FIGURE 3. 2-D definition for the burden surface.

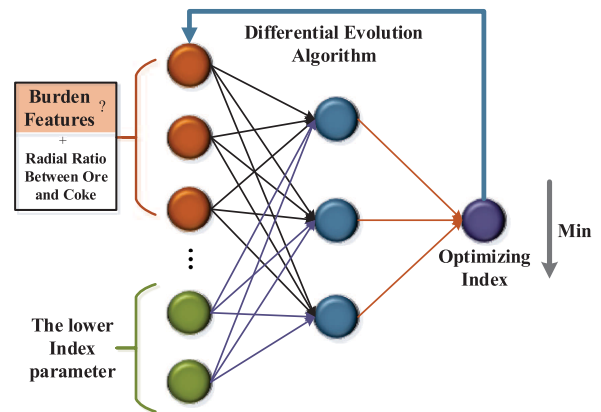


FIGURE 4. The optimization model.

the indicator parameters of the lower operations, such as the air temperature, air volume and oxygen enrichment, can also affect the operating performances [28] In the optimization model for the burden line, we should get rid of the impact of lower adjustment. Thus the lower indicator parameters are also set as the model inputs. However, they would not be the optimization variables during the optimization process. DE algorithm is employed to search for the features of burden line based on the optimal operating performances.

In the optimization model, we select the optimizing index that can present the operating condition of BF. The iron-making process of BF is complex and with many types of operating conditions. Here an integrated optimization index is selected, which constitutes with three individuals such that

(1) Gas utilization ratio. During the iron-making process, the gas utilization ratio(GUR) refers to the conversion efficiency of iron ore by the blast furnace gas. The improvement of GUR is the embodiment of the technological progress in BF operation. The calculation of GUR is as follows:

$$S = \frac{V(CO_2)}{V(CO_1) + V(CO_2)} \tag{7}$$

(2) Coke ratio. The coke ratio refers to the quality of the coke required for smelting each ton of pig iron. The coke ratio is one of the most important technical and economic indexes in BF production. Smaller coke ratio often means the higher efficiency. The calculation is as follows

$$R = \frac{m_a}{m_0} \quad (8)$$

where m_a is the quality of the coke, while m_0 represents the quality of pig iron.

(3) Permeability index. The permeability index is defined as the ratio of air volume(Q) and the total pressure difference(ΔP). It is a fast, intuitive and comprehensive parameter to reflect the status of BF production. The improvement of permeability index can ensure the stable operation of BF. The calculation is as follows.

$$T = \frac{Q}{P_2 - P_3} = \frac{Q}{\Delta P} \quad (9)$$

The above indicators can reflect the operating conditions of BF from different aspects^{29,30}. And the operators often pay different degrees of importance on the three indicators. Three indicators affect each other, resulting that the optimization model of burden surface is a trade-off optimization problem. For example, a blast furnace with a higher air permeability index often means a lower gas utilization rate, because the gas used for the reduction reaction is often easy to slip away. The degree of coke rate has a more or less impact on the permeability index. In addition, the scale of three indicators is different. The normalization is very necessary. Here we consider the following standardized variables

$$\begin{cases} \bar{S} = \frac{\|S_{max} - S\|}{S_{max} - R_{min}} \\ \bar{R} = \frac{R_{min} - R}{R_{min} - T_{max}} \\ \bar{T} = \frac{\|T_{max} - T\|}{T_{max}} \end{cases} \quad (10)$$

where S_{max} and T_{max} are the max or the expected values of the gas utilization ratio and the permeability index respectively, while R_{min} is the min or the expected value of coke ratio. Thus the total optimization index is as follows

$$P = w_1 \bar{S} + w_2 \bar{R} + w_3 \bar{T} \quad (11)$$

where w_1 , w_2 and w_3 are the weights on the different indicators.

The selection of weights is based on the pursuit of iron-making process in BF, which would be determined in advance [34]. In general, it should be satisfied that $w_1 + w_2 + w_3 = 1$. Then the optimization model for the optimal burden surface can be summarized as

$$\begin{aligned} \min P &= F(x_1, x_2, \dots, x_7, h; l) \\ s.t. &\begin{cases} x_{min}^i \leq x_i \leq x_{max}^i \\ h_{min} \leq h \leq h_{max} \end{cases} \end{aligned} \quad (12)$$

where x_i presents the features of burden line, while h_i is the radial ratio between ore and coke.

III. PRECISE CHARGING STRATEGY

In this section, we present the study on precise charging based on the optimal burden surface. The precise charging operation aims to achieve the optimal burden surface by the appropriate charging strategy, regardless of the shape of the basic burden surface. The precise charging is the goal of automation operation in iron-making process in BF, which can reduce the charging cost and achieve the purpose of energy-saving and emission reduction. The traditional charging rules contain two variables, the chute angle and rotation numbers. The sown burden volume is same on different locations on one burden ring. Unscrupulously, it is rough charging way. In the precise charging strategy, we add another additional variable into the charging rules, the throttle opening degree. The new charging rules are defined as follows

$$T = \{ \alpha \quad n \quad \gamma \} \quad (13)$$

where α and n are the chute angle and rotation numbers respectively, while γ represents the throttle opening degree.

Fig. 5 presents the precise burden charging scheme, including three main operating procedures: burden surface inspection, required burden volume calculation and precise charging operation. First, the 3D burden surface reconstruction is carried out based on the phased array radar detection technique, which can accurately obtain the point cloud data representing the height information of burden surface. The basic burden surface can be obtained. Second, based on the pre-set burden charging parameters, such as the chute angle and the number of rotations, the space motion model of the burden particles can be established, which can get the dropping points of burden particles on different charging stalls. We divide every burden charging stalls into four units. Combined the optimal burden surface shape, it is easy to calculate the required burden volume on each charging unit. Finally, the mapping relationship between throttle valve opening degree and required burden volume is established. By adaptively adjusting the opening of the throttle valve, the burden material with appropriate volume can be sprinkled in the correct position, and finally achieving the optimal burden surface.

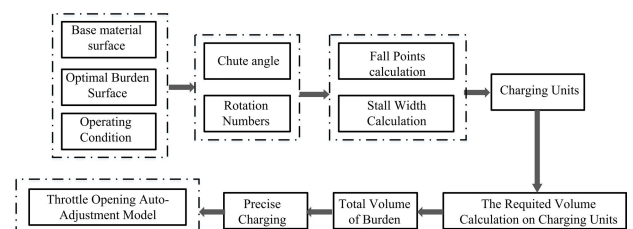


FIGURE 5. The precise charging scheme.

In the precise charging strategy, Fig. 6 puts forward the concept of charging units. Charging units refer to the fragmentation of one ring partition for burden surface. Based on the height of optimal burden surface, the required burden volume on different charging unit can be calculated.

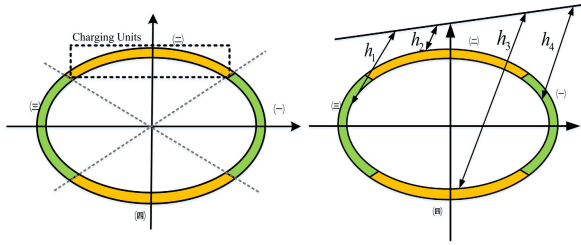


FIGURE 6. The calculation of required volume of burden on the charging units.

A. PHASED ARRAY RADAR DETECTION TECHNOLOGY

The industrial phased array radar detection system can accurately obtain the height information of the solid burden surface in the dark, high temperature and dusty harsh environment³¹. It is a kind of 3D burden surface detection device, which can receive the electromagnetic reflection echo signals of multi-bean spot, resulting to obtain almost the whole height information to the burden surface [32] The phased array radar detection system solve the bottleneck problem of less surface height data. Fig. 7 presents the phased array radar detection system, where Fig. 7(a) is the phased array radar device, while Fig. 7(b) present the point cloud data of burden surface.

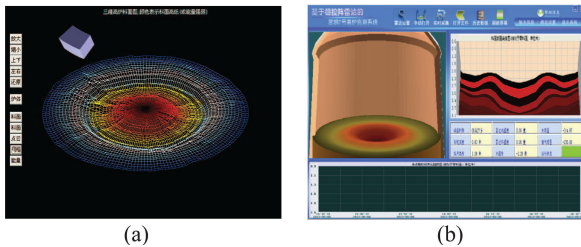


FIGURE 7. The phased array radar detection system. (a) The phased array radar device; (b) 3-D burden surface presentation. The color presents the heights of burden surface, or the strength of the energy.

B. THE CALCULATION OF PARTICLE FALLING POINT

The circular charging strategy is the most commonly used operation in BF. The chute, driven by the motor, spills the burden uniformly. The burden materials will be charged into the hoppers by the conveyor belts. During the discharge process, the burden will flow down through the flow control gate, low valve chamber, central throat tube to rotating chute. Then the rotating chute distributes the burden circumferentially onto the basic surface through the freeboard [33] Fig. 8 presents the burden movement trajectory model. The burden materials will pass through the flow control gate under a certain initial speed v_0 , which can be calculated as

$$v_0 = \frac{M}{\pi\rho\left(2S/L_s - d/2\right)^2} \tag{14}$$

where M is the actual mass flow rate through the throttle, kg/s . ρ is the bulk density of burden, kg/m^3 . S represents the

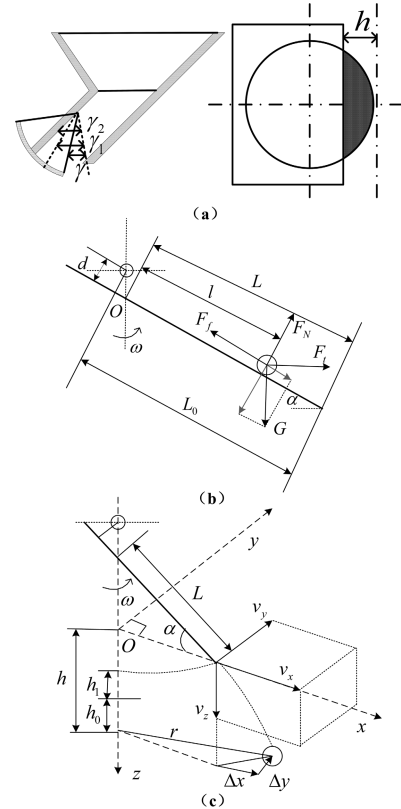


FIGURE 8. The burden movement trajectory model. (a) Cross section of the throttle; (b) The force analysis for the burden on the chute; (c) The force analysis for the burden in the free area.

projection area of the throttle outlet, m^2 . L_s is the edge length of the throttle, m , while d represents the average diameter of burden, m .

Here we consider the arc throttle, where the projection area S and edge length L_s of the throttle can be calculated as

$$\begin{cases} S = \frac{D^2}{4} \arccos\left(1 - \frac{2h}{D}\right) + \left(h - \frac{D}{2}\right) \sqrt{Dh - h^2} \\ L_s = D \arccos\left(1 - \frac{2h}{D}\right) + 2\sqrt{Dh - h^2} \end{cases} \tag{15}$$

where D is the diameter of central throat tube, m .

The effect on the bow height h by the throttle opening degree is serious, which can be obtained as

$$h = \begin{cases} r [\sin(\gamma_1) - \sin(\gamma_1 - \gamma)], & \gamma \in (0, \gamma_1) \\ r [\sin(\gamma_1) - \sin(\gamma - \gamma_1)], & \gamma \in (\gamma_1, \gamma_2) \\ D, & \gamma \in (\gamma_2, \gamma_{max}) \end{cases} \tag{16}$$

where r is the radius of throttle, m .

Then the burden particles will collide on the surface of the rotating chute through the central throat tube. The initial velocity of the particles moving on the rotating chute can be calculated as

$$v_1 = k\sqrt{v_0^2 + 2g(h_a + h_b)} \tag{17}$$

while k presents the correction factor of particles collision. h_a is the effective height from flow control gate to hanging point of rotating chute, m , while h_b is the effective height from the hanging point of rotating chute to colliding point of particles on the surface of the chute, m .

Fig. (b) presents the force analysis of the burden particles on the chute with a rotating speed of ω . The forces affecting the burden include the gravity, G ; the centrifugal force, $F_t = 4\pi^2 ml\omega^2 \cos(\alpha)$; the pressure force, $F_N = mg \sin(\alpha) - 4\pi^2 ml\omega^2 \cos^2(\alpha)$; the friction, $F_f = \mu F_N$, where l represents the moving distance of the burden particles on the rotating chute and μ is the friction coefficient. Then the accelerated speed of burden particles can be calculated as

$$a = \frac{dv_2}{dt} = g(\cos(\alpha) - \mu \sin(\alpha)) + 4\pi^2 l\omega^2 \cos(\alpha)(\sin(\alpha) + \mu \cos(\alpha)) \quad (18)$$

Then we can get the speed of burden particles at the end of the chute as

$$v_2 = \left(\frac{2g(\sin(\alpha) - \mu \cos(\alpha))L}{+4\pi^2 \omega^2 \cos(\alpha)(\cos(\alpha) + \mu \sin(\alpha))L^2} + (v_1 \sin(\alpha))^2 \right)^{1/2} \quad (19)$$

where $L = L_0 - d \tan(\alpha)$, and d is the vertical distance between the chute hanging point with the chute surface, m , while L_0 is the length of the chute, m . After the movement on the chute, the burden particles are discharged through the freeboard. The particle will be affected by many kinds of forces, mainly including the gravitational force, the drag force, and the buoyancy force [34]. The 3D coordinate system is established in the freeboard as shown in (c) of Fig. 8, where the sub-speeds of three directions can be calculated as

$$\begin{cases} v_{x,2} = v_2 \cos(\alpha) \\ v_{y,2} = \pi \omega L \cos(\alpha) \\ v_{z,2} = v_2 \sin(\alpha) \end{cases} \quad (20)$$

We present the meaning of the main symbols used in the following deviation. $v_{g,x}$, $v_{g,y}$ and $v_{g,z}$ represent the gas flow velocities in the x , y and z coordinates respectively, m/s ; ρ_g is the gas density, kg/m^3 ; V_p is the particle volume, m^3 ; d_p is the particle diameter, m ; μ_g is the gas viscosity coefficient, $Pa \cdot s$; ϕ is the shape fraction; a_x , a_y and a_z are the accelerated velocities of the particle in the x , y and z coordinates respectively, m/s^2 ;

The particles depending in the freeboard are affected by the buoyancy force, which is represented by F_b , $F_b = \rho_g g V_p$. The drag force in every coordinate can be calculated as $F_{d,i} = C(v_{i,2} - v_{g,i})^2$, $i = x, y, z$. Then one can get the following three equations to describe the movements of the particle in the freeboard.

$$\begin{cases} -ma_x = F_{d,x} \\ -ma_y = F_{d,y} \\ ma_z = mg - F_{d,z} - F_b \end{cases} \quad (21)$$

The coefficient of the drag force is given as follows:

$$C = \frac{1}{2} \left[1 + b_1 Re^{b_2} + \frac{b_3 Re}{b_4 + Re} \right] \frac{\pi r^2}{8} \rho_g \quad (22)$$

where

$$\begin{cases} b_1 = \exp(2.3288 - 6.4581\phi + 2.4486\phi^2) \\ b_2 = 0.0964 + 0.5566\phi \\ b_3 = \exp(4.905 - 13.8944\phi + 18.4222\phi^2 - 10.1599\phi^3) \\ b_4 = \exp(1.4681 + 12.2584\phi - 20.7322\phi^2 + 15.8855\phi^3) \end{cases} \quad (23)$$

and

$$Re = \frac{\rho_g d_p |v - v_g|}{\mu_g} \quad (24)$$

Based on the interval width division, one can obtain the height of the burden on every interval. Then one can divide the interval into four parts. This division is useful for the following introduction of precise charging strategy.

C. PRECISE CHARGING OPERATION

This subsection designs the precise charging strategy, which aims to charge the appropriate volume of burden on the corresponding charging units. The auto-adjustment model of the opening degree of the throttle is established. The opening degree of throttle controls the cross sectional area of burden flowing, and thus control the burden volume per unit time. It is important to establish the relationship model between the required volume of burden on the four charging units on one interval and the opening degree of throttle.

Fig. 9 presents the relationship between the throttle opening degree and the projection area, where one can see the projection area increases monotonically with the opening degree of the throttle until the maximum opening degree. Suppose the chute rotates at the speed of ω , The time passing the j th charging unit on the i th surface stall can be calculated as

$$\Delta t_{i,j} = \frac{2\pi}{4\omega} \quad (25)$$

Within this time period, the burden volume out of the throttle can be calculated as

$$V_{i,j} = n_i \cdot v_0 \Delta t_{i,j} S \quad (26)$$

where n_i represents the rotation number of the i th charging stall.

During the charging process, the adjustment rule of the throttle opening degrees is based on the required burden volume, which meets the need of precise charging.

IV. SIMULATION RESULTS

In this section, we present the simulation results based on the real industrial data of BF with $2500 m^3$ volume. There are three main simulations. The first refers to the calculation of optimal burden surface shape based on the historical phased array radar detection data. Then we calculate the required

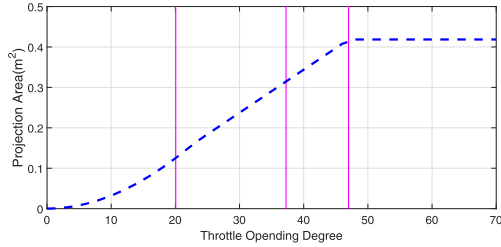


FIGURE 9. The relationship between the throttle opening degree and the projection area.

burden volume on the charging units based on the burden surface division strategy. In the end, the precise charging operation results are presented. Many relevant parameters of the bell-less top charging equipment and the calculation of interval width are presented in the above section. We list the main parameters in Table 1. Table 2 presents the charging rules, including the chute angle and its rotation numbers for charging ore and coke. In order to ensure the fairness of the simulation comparison test, all the simulations have been conducted in Matlab 7.8.0(2009a) running on a desktop PC with AMD Athlon(tm) X2 250 processor, 3.00-GHz CPU and 2G RAM.

TABLE 1. The simulation parameters.

Parameter	Value	Unit	Parameter	Value	Unit
N	9	—	d	9	m
r	0.55	m	λ_f	0.85	—
λ	0.35	m	k	0.75	—
h_a	3.80	m	h_b	5.52	—
D_0	0.65	m	g	9.8	m/s^2
ρ	1050	m/s^2	ω	0.78	rad/s
μ	0.5	—	L_0	4.5	m
μ_g	3×10^{-5}	—	ρ_g	0.8	kg/m^3
φ	0.72	—	d_p	47.5	mm
D	0.73	m	R	0.73	m

TABLE 2. The charging rules.

Stalls	1	2	3	4	5	6	7	8	9
Chute angle	39	37	35	33	31	29	27	24	21
Rotation numbers(Ore)	2	2	3	3	3	3	2	2	0
Rotation numbers(Coke)	3	2	2	2	2	3	3	3	2

A. 3D BURDEN SURFACE RECONSTRUCTION AND OPTIMAL BURDEN SURFACE MODEL

Here we present the simulation of 3D burden reconstruction and the optimal burden surface model based on the real phased array radar detection data. The operating environment of iron-making process is complex, resulting that burden surface detection data is often contaminated by noise. It is important and necessary to make denoising to the raw data. Fig. 10 presents 3D dot graph of blast furnace surface data,

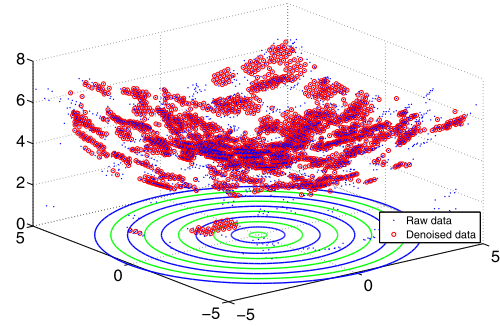


FIGURE 10. Phased array radar data.

where the blue real points are the raw detection data, while the red circles represent the remained data after denoising process. The detected points can cover the whole burden surface, and present the rough shape of burden surface.

In the burden surface optimization model, we make the regression model between the surface shape and the comprehensive performance index based on ELM algorithm. Here two indicator variables are employed, gas utilization ratio and permeability index, which are mutually exclusive in a sense. In general, higher gas utilization ratio means the gas has been fully reacted, which corresponds to worse permeability index. When the gas is easy to erupt, gas utilization ratio means is relatively lower, corresponding to better permeability index. In the simulation experiment, in order to avoid the weighted bias caused by different data dimensions, the data was standardized in the data preprocessing stage. We employ the random sampling method to divide the data into training set and testing set at a ratio of 4:1. In order to verify the effectiveness of the ELM algorithm in processing blast furnace data, SVM and BP algorithms are also employed to conduct the simulation experiments. In order to make the comparison results more convincing, we adopt the k -fold cross-validation method ($k = 10$) and carry out simulation experiments 50 times, and take the average values as the final simulation results.

According to the ELM algorithm theory, the fitting effect of the ELM algorithm will gradually become better as the number of hidden nodes increases. The corresponding training time will also increase, while facing the risk of overfitting. Fig. 11 and 12 present the simulation results of training error, testing error and training time with the increase of number of hidden nodes using partial simulation data, which provide good support for choosing the number of hidden nodes. From the simulation results we can see, that as the number of hidden nodes increases, the training accuracy and testing accuracy are improved, and at the same time, the training time also gradually increases. When the number of hidden nodes increased to about 1500, the testing error reaches the minimum, and increases later, which shows that this is the critical point of overfitting. In this way, the appropriate number of hidden nodes can be selected accurately.

Fig. 13 and Fig. 14 present the simulation results for the regression of gas utilization ratio and permeability index

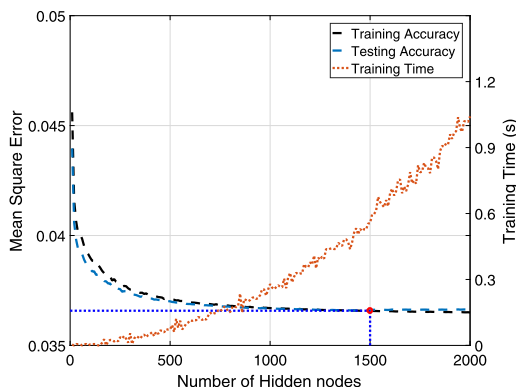


FIGURE 11. Simulation accuracy and training time with the increase of number of hidden nodes (gas utilization ratio).

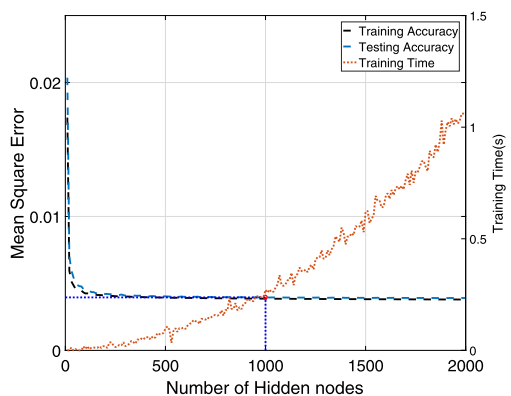


FIGURE 12. Simulation accuracy and training time with the increase of number of hidden nodes (permeability index).

based on ELM, SVR and BP algorithms. For ELM and BP algorithms, we select the same number of hidden nodes based on simulation results of Fig. 11 and 12. The number of hidden nodes is set to 1500 for gas utilization ratio regression, while 1000 for permeability index regression. And for SVM, the popular Gaussian kernel function $K(u, v) = \exp(-\gamma \|u - v\|^2)$ is used. It is known that the performance of SVM is sensitive to the combination of (C, γ) . We apply 50 different values of C and 50 different values of γ , resulting in a total of 2500 pairs of (C, γ) , and the best parameter pair is selected. In order to make the simulation results look clearer, we zoomed in on the local area. From the simulation results we can see that, compared with the SVR and BP algorithms, the ELM algorithm performs better when fitting blast furnace production data. In addition, the blast furnace production furnace conditions are changeable, and the data changes seriously over time. The ELM algorithm can capture data changes and achieve high-precision data fitting.

In addition to carrying out qualitative simulations, we also calculate the quantitative results of the regression experiments. Table 3 and Table 4 present the simulation results,

TABLE 3. The simulation results for gas utilization ratio regression.

Algorithm Parameters	Time (s)		Accuracy	
	Training	Testing	Training	Testing
BP (3, 1500)	1.235	0.542	0.054(±0.005)	0.061(±0.006)
SVR ($2^{10}, 2^4$)	1.356	0.895	0.101(±0.004)	0.105 (±0.005)
ELM 1500	0.523	0.534	0.037(±0.003)	0.037(±0.003)

TABLE 4. The simulation results for permeability index regression.

Algorithm Parameters	Time (s)		Accuracy	
	Training	Testing	Training	Testing
BP (3, 1000)	1.244	0.541	0.052(±0.005)	0.060(±0.005)
SVR ($2^{12}, 2^5$)	1.366	0.885	0.100(±0.004)	0.101(±0.005)
ELM 1000	0.526	0.543	0.034(±0.003)	0.036(±0.003)

where the columns named “Parameters” show the optimal hyperparameter selection for different algorithms. Taking Table 3 as an example, (3, 1500) in the BP algorithm means that the network structure has three layers and the number of hidden nodes is 1500; $(2^{10}, 2^4)$ is the optimal value for the parameter pair of (C, γ) in SVR algorithm; 1500 in ELM algorithm represents the number of hidden nodes. From the simulation results we can see that, relatively speaking, ELM algorithm achieves the best trade-off between training time and simulation accuracy, which can meet the real needs of iron-making production in BF.

We select the production data of the BF in a certain charging period, and employ the DE algorithm to find the optimal material surface. Fig. 15 presents the simulation result of DE algorithm for the search to the optimal burden surface. With the increase of iterative generations, the performance index reduces gradually, and tends to be stable. Table 5 presents the optimal features of burden surface and the radial ratio between the ore and coke. In iron-making production of BF, it is difficult to determine the benefits of an operation in time. The determination of the optimal burden surface follows the same rule. The best way to determine whether the burden surface shape is appropriate is to rely on expert experience. We feed back the shape of the burden surfaces under different operating conditions obtained by the proposed model to experts with rich operating experience, and they are professionally recognized.

B. THE REQUIRED BURDEN VOLUME CALCULATION ON CHARGING UNITS

The calculation of the required burden volume on charging units is the important element of precise charging process. In this paper, we obtain the width of ring partition on burden surface through the determination of falling points of the burden particles on different charging stalls. Fig. 16 presents the results of falling points, where the width of ring partition can be calculated based on the spacing between the red and blue lines. From the drop points of the burden material on different stalls, we can see that, the falling points are not on concentric circles, which is due to the asymmetry of the charging device.

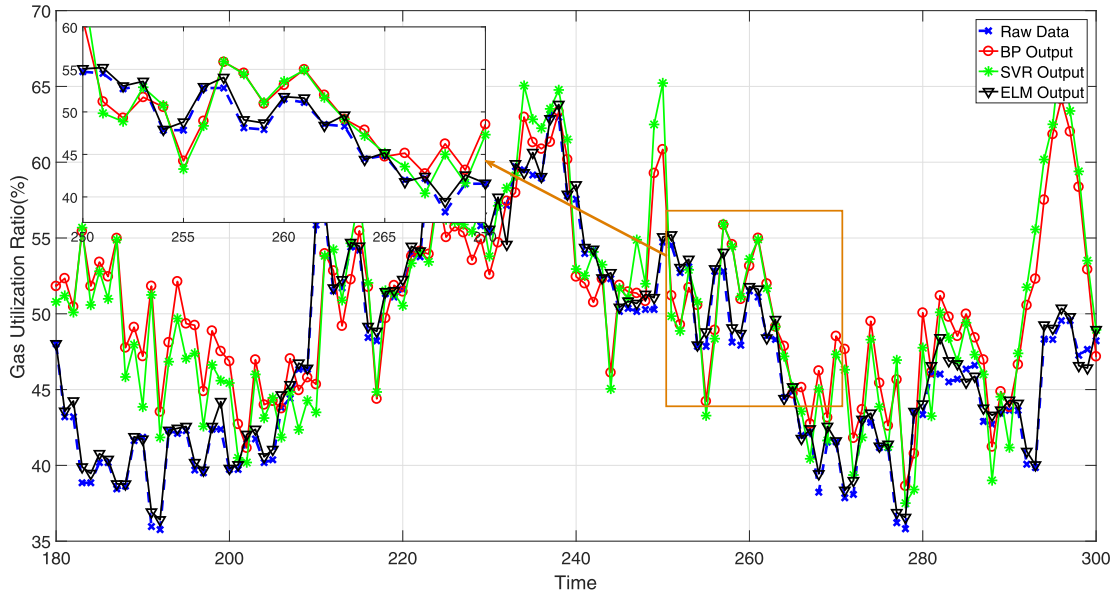


FIGURE 13. ELM regression result for gas utilization ratio.

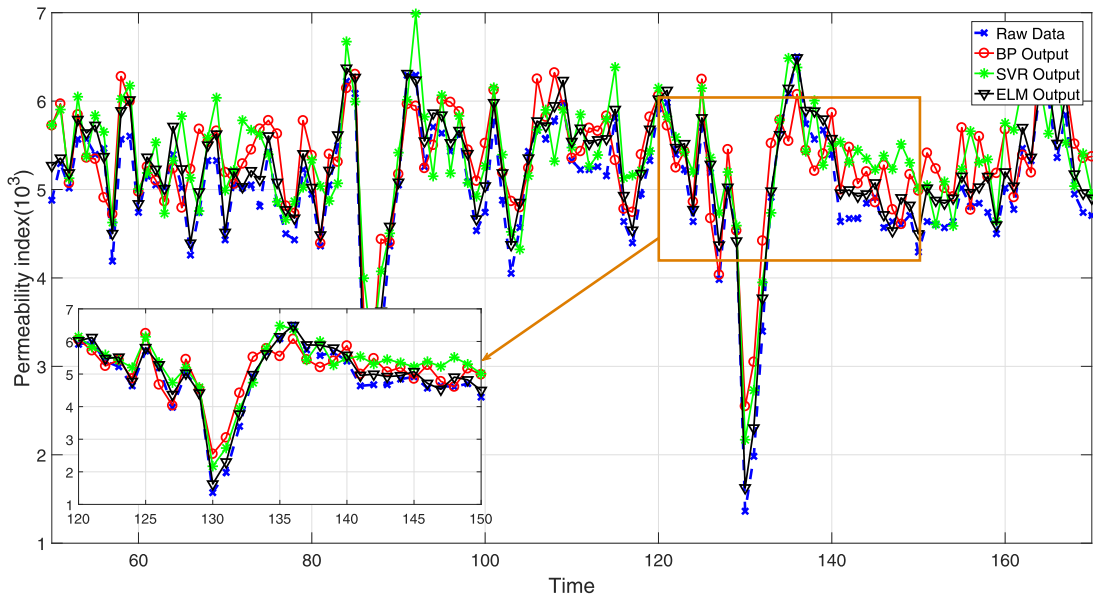


FIGURE 14. ELM regression result for permeability index.

TABLE 5. The optimal burden surface results.

Burden surface features							Radial ratio between ore and coke								
h_1	h_2	l_1	l_2	α	β	γ	1	2	3	4	5	6	7	8	9
0.845	0.594	1.300	1.460	19.700	24.830	-6.730	1.025	1.031	1.258	1.309	1.309	1.358	1.333	1.356	1.357

It is very easy to calculate the required burden material volume after obtaining the optimal burden surface shape and the dropping points distribution. Table 6 presents the required burden volume on different charging units subject to the coke and ore. Fig. 19 shows the information of the basic burden material surface and required burden material for 9 stalls.

The required burden material volume among different stalls reflects a significant difference. In the charging process, it is wrong to treat charging operations at different positions equally. The charging parameters about the auto-adjustment of the throttle opening degree and the chute rotation speed would be determined based on the results of Table 5.

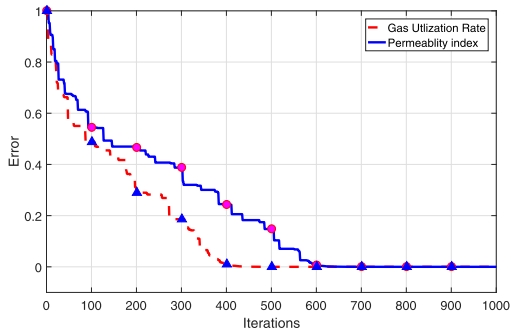


FIGURE 15. The regression results of DE algorithm.

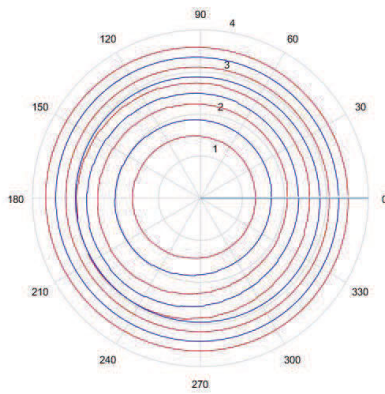


FIGURE 16. The falling points of the burden particles.

C. THE PRECISE CHARGING OPERATION

Based on the required burden volume results from Table 6, one can obtain the auto-adjustment model of the throttle

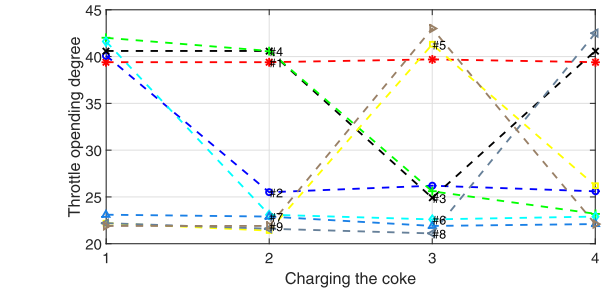


FIGURE 17. The falling points of the burden particles.

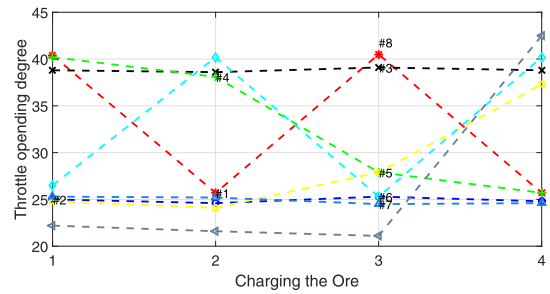


FIGURE 18. The falling points of the burden particles.

opening degrees. It is worth mentioning that there is no analytical solution for the relationship between the required burden volume and the throttle opening degrees. However, there is a one-to-one correspondence between them, obtained from Fig. 9. Through computer simulation and interpolation operation, we can easily obtain the throttle opening degrees corresponding to different burden material volumes.

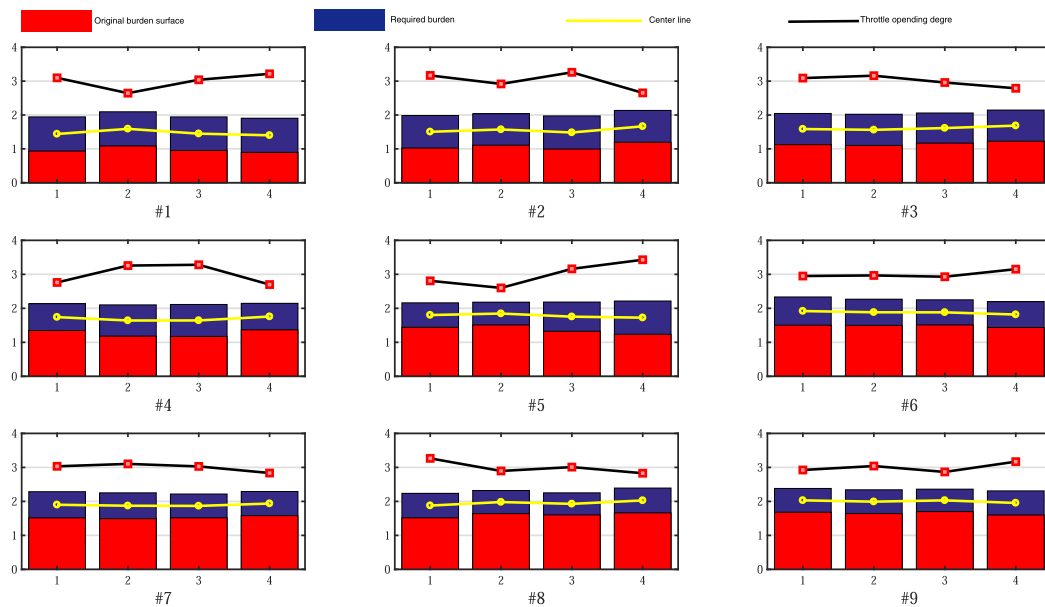


FIGURE 19. The precise charging operation simulation. The red bar represents the original burden surface; the blue bar represents the required burden volume; the yellow curve represents the center points of the required burden volume; the black curve represents the throttle opening degrees.

TABLE 6. The required burden volume.

Interval	The Required Burden Volume (m^3)								Sum	
	1		2		3		4			
	O	C	O	C	O	C	O	C	O	C
1	1.03	1.01	1.04	1.01	1.02	0.99	1.04	1.01	4.12	4.02
2	0.99	0.96	0.96	0.93	1.01	0.98	0.97	0.94	3.93	3.81
3	1.15	0.92	1.16	0.92	1.13	0.89	1.15	0.92	4.59	3.65
4	1.05	0.79	1.19	0.92	1.21	0.94	1.04	0.78	4.49	3.43
5	0.97	0.72	0.92	0.67	1.21	0.86	1.23	0.98	4.23	3.23
6	1.10	0.83	1.05	0.77	1.01	0.74	1.05	0.76	4.21	3.10
7	1.01	0.77	1.00	0.76	0.95	0.70	0.96	0.71	3.92	2.94
8	0.97	0.72	0.93	0.68	0.89	0.65	0.98	0.73	3.77	2.78
9	0.70	0.70	0.70	0.70	0.66	0.66	0.71	0.71	2.77	2.77
Sum	9.22	7.42	9.20	7.36	9.33	7.41	9.39	7.54	37.02	29.73

Fig. 17 and Fig. 18 present the changing results of the throttle opening degrees for the ore and coke respectively. The charging operation in BF is a continuous operation process. The rules of opening values of the throttle would be set in advance, which can make sure to spill the appropriate volume of burden to the correct areas.

Fig. 19 presents the precise charging operation simulation results. We have validated the proposed precise charging model on a real blast furnace. Based on the radar detection technology, we obtain the real burden surface shape, which is in line with the optimal burden surface.

V. CONCLUSION

The iron-making production in BF is an extremely complex industrial process, in which the charging operation plays an important role in high-quality development. A general precise burden charging strategy is proposed. It can realize the optimal burden surface shape by adaptively adjusting the opening degree of the throttle valve on the basic burden surface, where the optimal burden surface can be obtained through the index optimizing strategy. Simulation experiments using real production data in blast furnaces verify the effectiveness of the precise burden charging model. Here we present two hot open problems for future research.

(1) For the ELM algorithm applied in the regression model of iron-making production index, how to determine the number of hidden nodes appropriately is a topic worth studying.

The number of hidden nodes affects the fitting performance of the ELM algorithm. Although there are many methods to study how to determine the number of hidden nodes in the ELM algorithm, there is still no unified specification. In most cases, we can only use experimental simulation to determine the appropriate number of nodes.

(2) The iron-making in BF is an online production process. It is necessary to build an online, real-time updated regression model.

Iron-making production in blast furnace is a continuous process. Production status changes over time. Therefore, it is necessary to establish an online regression model for the production index during iron-making process. OS-ELM algorithm is the basic framework of online ELM algorithm.

However, after our verification, the OS-ELM algorithm does not work well. The reason is that, expect for the time-series characteristics, there is also the large delay during blast furnace production data. So, how to process the production data online based on ELM framework is an open problem.

REFERENCES

- [1] S. Hutangkabodee, Y. Zweiri, L. Seneviratne, and K. Althoefer, "Soil parameter identification and driving force prediction for wheel-terrain interaction," *Int. J. Adv. Robot. Syst.*, vol. 5, no. 4, p. 35, Nov. 2008.
- [2] X. Su, S. Zhang, Y. Yin, and W. Xiao, "Prediction model of permeability index for blast furnace based on the improved multi-layer extreme learning machine and wavelet transform," *J. Franklin Inst.*, vol. 355, no. 4, pp. 1663–1691, Mar. 2018.
- [3] H. Saxen, C. Gao, and Z. Gao, "Data-driven time discrete models for dynamic prediction of the hot metal silicon content in the blast furnace—A review," *IEEE Trans. Ind. Informat.*, vol. 9, no. 4, pp. 2213–2225, Nov. 2013.
- [4] J.-I. Park, H.-J. Jung, M.-K. Jo, H.-S. Oh, and J.-W. Han, "Mathematical modeling of the burden distribution in the blast furnace shaft," *Met. Mater. Int.*, vol. 17, no. 3, pp. 485–496, Jun. 2011.
- [5] J. Xu, S. Wu, M. Kou, L. Zhang, and X. Yu, "Circumferential burden distribution behaviors at bell-less top blast furnace with parallel type hoppers," *Appl. Math. Model.*, vol. 35, no. 3, pp. 1439–1455, Mar. 2011.
- [6] F. I. Gamero, J. Colomer, J. Meléndez, and P. Warren, "Predicting aerodynamic instabilities in a blast furnace," *Eng. Appl. Artif. Intell.*, vol. 19, no. 1, pp. 103–111, Feb. 2006.
- [7] L. Jian and C. Gao, "Binary coding SVMs for the multiclass problem of blast furnace system," *IEEE Trans. Ind. Electron.*, vol. 60, no. 9, pp. 3846–3856, Sep. 2013.
- [8] J.-S. Zeng and C.-H. Gao, "Improvement of identification of blast furnace ironmaking process by outlier detection and missing value imputation," *J. Process Control*, vol. 19, no. 9, pp. 1519–1528, Oct. 2009.
- [9] H. Zhao, M. Zhu, P. Du, S. Taguchi, and H. Wei, "Uneven distribution of burden materials at blast furnace top in bell-less top with parallel bunkers," *ISIJ Int.*, vol. 52, no. 12, pp. 2177–2185, 2012.
- [10] J. An, J. Yang, M. Wu, J. She, and T. Terano, "Decoupling control method with fuzzy theory for top pressure of blast furnace," *IEEE Trans. Control Syst. Technol.*, vol. 27, no. 6, pp. 2735–2742, Nov. 2019.
- [11] M. Ramacciotti, M. Milazzo, F. Leoni, S. Roccella, and C. Stefanini, "A novel shared control algorithm for industrial robots," *Int. J. Adv. Robot. Syst.*, vol. 13, no. 6, pp. 1–10, Dec. 2016.
- [12] C. A. Tokognon, B. Gao, G. Y. Tian, and Y. Yan, "Structural health monitoring framework based on Internet of Things: A survey," *IEEE Internet Things J.*, vol. 4, no. 3, pp. 619–635, Jun. 2017.
- [13] S. Liu, Z. Zhou, K. Dong, A. Yu, D. Pinson, and J. Tsalapatis, "Numerical investigation of burden distribution in a blast furnace," *Steel Res. Int.*, vol. 86, no. 6, pp. 651–661, Jun. 2015.
- [14] Q. Zhu, C.-L. Lü, Y.-X. Yin, and X.-Z. Chen, "Burden distribution calculation of bell-less top of blast furnace based on multi-radar data," *J. Iron Steel Res. Int.*, vol. 20, no. 6, pp. 33–37, Jun. 2013.
- [15] X. Liu, L. Chen, H. Feng, X. Qin, and F. Sun, "Constructal design of a blast furnace iron-making process based on multi-objective optimization," *Energy*, vol. 109, pp. 137–151, Aug. 2016.
- [16] F. Pettersson, H. Saxén, and K. Deb, "Genetic algorithm-based multi-criteria optimization of ironmaking in the blast furnace," *Mater. Manuf. Processes*, vol. 24, no. 3, pp. 343–349, Feb. 2009.
- [17] C. C. Hua, Y. J. Wang, J. P. Li, and Y. G. Tang, "Multi-objective optimization model for blast furnace production and ingredients based on NSGA-II algorithm," *CIESC J.*, vol. 67, no. 3, pp. 1040–1047, 2016.
- [18] X. Hao, G. Du, Z. Xie, and F. Shen, "Application of fuzzy causal classification model for forecasting coke ratio in blast furnace," *J. Northeastern Univ.*, vol. 26, no. 4, pp. 363–366, 2005.
- [19] V. V. Horupakha, Y. S. Semenov, E. I. Shumelchik, and S. V. Vashchenko, "Influence of transient blast furnace conditions on the temperature in the cooling system," *Steel Transl.*, vol. 49, no. 6, pp. 397–401, Jun. 2019.
- [20] G.-B. Huang, Q.-Y. Zhu, and C.-K. Siew, "Extreme learning machine: Theory and applications," *Neurocomputing*, vol. 70, nos. 1–3, pp. 489–501, 2006.
- [21] R. Storn and K. Price, "Differential evolution—A simple and efficient heuristic for global optimization over continuous spaces," *J. Global Optim.*, vol. 11, no. 4, pp. 341–359, 1997.

- [22] G.-B. Huang, H. Zhou, X. Ding, and R. Zhang, "Extreme learning machine for regression and multiclass classification," *IEEE Trans. Syst., Man, Cybern., B, Cybern.*, vol. 42, no. 2, pp. 513–529, Apr. 2012.
- [23] H.-G. Zhang, S. Zhang, and Y.-X. Yin, "A novel improved ELM algorithm for a real industrial application," *Math. Problems Eng.*, vol. 2014, Jan. 2014, Art. no. 824765.
- [24] R. Fletcher, *Practical Methods of Optimization*, vol. 33, no. 7. Hoboken, NJ, USA: Wiley, 2013, pp. 675–676.
- [25] J. Brest, S. Greiner, B. Boskovic, M. Mernik, and V. Zumer, "Self-adapting control parameters in differential evolution: A comparative study on numerical benchmark problems," *IEEE Trans. Evol. Comput.*, vol. 10, no. 6, pp. 646–657, Dec. 2006.
- [26] A. K. Qin, V. L. Huang, and P. N. Suganthan, "Differential evolution algorithm with strategy adaptation for global numerical optimization," *IEEE Trans. Evol. Comput.*, vol. 13, no. 2, pp. 398–417, Apr. 2009.
- [27] J. Vesterstrom and R. Thomsen, "A comparative study of differential evolution, particle swarm optimization, and evolutionary algorithms on numerical benchmark problems," in *Proc. Congr. Evol. Comput.*, vol. 2, Jun. 2004, pp. 1980–1987.
- [28] X. F. Dong, D. Pinson, S. J. Zhang, A. B. Yu, and P. Zulli, "Gas-powder flow in blast furnace with different shapes of cohesive zone," *Appl. Math. Model.*, vol. 30, no. 11, pp. 1293–1309, Nov. 2006.
- [29] J. An, F. Yin, M. Wu, J. She, and X. Chen, "Multi-source wind speed fusion method for short-term wind power prediction," *IEEE Trans. Ind. Informat.*, early access, Jul. 3, 2020, doi: [10.1109/tii.2020.3006928](https://doi.org/10.1109/tii.2020.3006928).
- [30] H. Wang, C. Sheng, and X. Lu, "Knowledge-based control and optimization of blast furnace gas system in steel industry," *IEEE Access*, vol. 5, pp. 25034–25045, 2017.
- [31] M. D. Buhari, G. Y. Tian, and R. Tiwari, "Microwave-based SAR technique for pipeline inspection using autofocus range-Doppler algorithm," *IEEE Sensors J.*, vol. 19, no. 5, pp. 1777–1787, Mar. 2019.
- [32] C. Xianzhong, Y. Yixin, H. Qingwen, L. Xiaoli, Z. Menghui, and L. Kangli, "A design of phased array antenna based on the Vivaldi antenna," in *Proc. 2nd Int. Conf. Ind. Inf. Syst.*, Mangalore, India, Jul./Aug. 2010, pp. 334–337.
- [33] G. Zhao, S. Cheng, W. Xu, and C. Li, "Comprehensive mathematical model for particle flow and circumferential burden distribution in charging process of bell-less top blast furnace with parallel hoppers," *ISIJ Int.*, vol. 55, no. 12, pp. 2566–2575, 2015.
- [34] Z.-J. Teng, S.-S. Cheng, P.-Y. Du, and X.-B. Guo, "Mathematical model of burden distribution for the bell-less top of a blast furnace," *Int. J. Minerals, Metall., Mater.*, vol. 20, no. 7, pp. 620–626, Jul. 2013.



HAIGANG ZHANG (Member, IEEE) received the B.S. degree from the University of Science and Technology Liaoning, in 2012 and the Ph.D. degree from the School of Automation and Electrical Engineering, University of Science and Technology Beijing, in 2018. He is currently working with the Institute of Applied Artificial Intelligence of the Guangdong-Hong Kong-Macao Greater Bay Area, Shenzhen Polytechnic. His research interests include machine learning, image process, and biometrics recognition.



SHAOLUN SUN (Member, IEEE) is currently pursuing the Ph.D. degree with the School of Automation and Electrical Engineering, University of Science and Technology Beijing. His research interests include machine learning, iron-making, and robust control.



SEN ZHANG (Member, IEEE) received the Ph.D. degree in electrical engineering from Nanyang Technological University, in 2005. She is currently working as a Postdoctoral Research Fellow with the National University of Singapore and a Lecturer with Singapore Polytechnic. She is also an Associate Professor with the School of Automation and Electrical Engineering, University of Science and Technology Beijing. Her research interests include ELM, target tracking, and estimation theory.

• • •